ELSEVIER

International Journal of Heat and Fluid Flow 21 (2000) 727–734

International Journal of
HEAT AND
FLUID FLOW

www.elsevier.com/locate/ijhff

Numerical investigation of condensing steam flow in boundary layers

A.J. White

School of Engineering, University of Durham, South Road, Durham DH1 3LE, UK

Received 2 August 1999; accepted 25 March 2000

Abstract

The paper describes a numerical method for the prediction of condensing steam flow within compressible boundary layers. The method is based on a simple stream function technique, which enables straightforward integration of the nucleation and droplet growth equations in a Lagrangian frame of reference. Calculations show how viscous dissipation and reduced expansion rate within a typical boundary layer influence nucleation and growth, leading to droplet radii and size distributions that differ substantially from those predicted in inviscid flow. The impact of condensation on temperature and velocity profiles, and the implications for thermodynamic loss are also considered.

Keywords: Condensation; Wet-steam; Droplets; Boundary layers

1. Introduction

Formation of droplets by spontaneous condensation of water vapour is of practical importance in a number of engineering fields, including the flow of steam in low pressure turbines, the flight of aircraft in humid air and various chemical engineering applications. Wet-steam research for turbine flows has focussed on the problems of blade erosion, thermodynamic and mechanical wetness losses, and the influence of the condensation process on blade aerodynamics. All of these effects are strongly influenced by the size of fog-droplets formed by spontaneous nucleation (Gyarmathy, 1963) and it is therefore important that all the processes governing the formation and growth of droplets are properly understood and accounted for.

During the past decade, a number of calculation procedures for inviscid condensing flow have appeared in the literature, including the methods of Bakhtar and So (1991) and White and Young (1993) for pure steam, and of Schnerr and Dohrmann (1988) for moist air. Such methods are able to correctly calculate pressure distributions and average droplet sizes for nozzle and turbine cascade flows. However, optical measurements on operating turbines suggest that droplets are present with a broad range of sizes (Walters, 1988) which contrasts strongly with the narrow spectra predicted by inviscid calculations. A number of factors may contribute to the broad size range (including the wake-chopping effects discussed by Bakhtar and Heaton, 1988, Guha and Young, 1994, and others) and it is likely that viscous effects play some rôle. Calculations including viscous effects are not common; two notable examples are the boundary layer calculations described in papers by Studziński et al. (1979), and Schnerr et al. (1992). Both methods use a mono-dispersed population of droplets to model the liquid phase. Results presented in the current paper suggest, however, that viscous effects lead to prolonged and secondary nucleations which can only be accurately modelled using a polydispersion of droplet sizes.

Compared with inviscid flow, boundary layer effects are likely to influence the condensation process in two principal ways. Firstly, fluid particles passing through the boundary layer experience approximately the same spatial variations in pressure, but travel more slowly than in the free-stream. Expansion rates are thus slower, leading to smaller departures from equilibrium. Secondly, whereas nucleation within inviscid flow is usually terminated by the release of latent heat from growing droplets, viscous heating and the conduction of heat from hotter zones may prematurely truncate the nucleation process in boundary layer flow. Both effects would tend to reduce the number of droplets nucleated, leading to larger droplet sizes once equilibrium conditions have been established. In addition to these differences, condensation heat release may substantially modify the pressure distribution at the edge of the boundary layer, resulting in different velocity profiles and integral properties to those observed in single-phase flow (Schnerr et al., 1992). The calculation method presented here has been used to investigate the above-mentioned effects in detail and also to determine how temperature profiles and entropy generation are affected by the condensation process. No detailed experimental data currently exist for condensation within boundary layers but the ability of the current scheme to predict boundary layer effects has been comprehensively tested for standard single-phase cases, and the nucleation and droplet-growth routines have been validated elsewhere by extensive comparison with nozzle and

E-mail address: alexander.white@durham.ac.uk (A.J. White).

0142-727X/00/$ - see front matter
PII: S0142-727X(00)00030-8

Notation

c_{pv}	specific isobaric heat capacity of vapour
h	specific enthalpy
h_o	specific stagnation enthalpy of mixture
J	nucleation rate per unit mass of mixture
m_i	group-i droplet mass
n_i	number of group-i droplets per unit mass of mixture
p	pressure
Pr	Prandtl number
q_y	heat flux in y direction
r	wall temperature recovery factor (defined in text)
R	gas constant for H_2O per unit mass
r_i	radius of group-i droplets
r_*	Kelvin–Helmholtz critical radius
S	entropy/source term
t	time
T	temperature
u, v	velocity components
x, y	spatial coordinates
y	wetness fraction
ΔT	vapour subcooling, $(T_s - T_v)$
λ	thermal conductivity of vapour
μ	dynamic viscosity of vapour
ψ	stream function
ρ	density
τ	shear stress

Subscripts

f	liquid phase
i	group-i droplets/streamwise location
s	saturation quantity
t	turbulent values
v	vapour phase
∞	free-stream values

Unsubscripted quantities refer to mixture values where appropriate.

turbine cascade data (White and Young, 1993 and White et al., 1996).

2. Governing equations

2.1. Boundary layer equations for condensing flow

Fog droplets produced by spontaneous condensation are sufficiently small that they may be assumed to follow vapour-phase streamlines without slip. With this assumption, the conservation equations for the vapour-droplet mixture as a whole are identical to the corresponding equations for single phase-flow. For steady, compressible flow on a flat surface, the mass continuity, momentum and energy equations (with the usual boundary layer approximations) are respectively:

$$\frac{\partial}{\partial x}(\rho u) + \frac{\partial}{\partial y}(\rho v) = 0, \tag{1}$$

$$\rho u \frac{\partial u}{\partial x} + \rho v \frac{\partial u}{\partial y} = \frac{\partial \tau}{\partial y} - \frac{\mathrm{d}p}{\mathrm{d}x}, \tag{2}$$

$$\rho u \frac{\partial h_o}{\partial x} + \rho v \frac{\partial h_o}{\partial y} = \frac{\partial}{\partial y}(u\tau - q_y), \tag{3}$$

where τ is the shear stress, q_y is the local heat flux normal to the main flow direction, and $h_o = h + \frac{1}{2}u^2$ is the mixture specific stagnation enthalpy neglecting the very small contribution from the normal velocity. Two-phase effects enter into these equations through the density, ρ, and enthalpy, h. These are non-equilibrium mixture quantities and therefore depend on the mass fraction of liquid and on the vapour subcooling, defined as $\Delta T = T_s - T_v$, where T_s and T_v are the saturation and vapour temperatures, respectively. Mathematical closure of Eqs. (1)–(3) requires expressions for formation and growth of the liquid phase as described below.

Turbulence effects are included by means of an eddy viscosity and eddy conductivity

$$\tau = (\mu + \mu_t)\frac{\partial u}{\partial y} \text{ and } q_y = -(\lambda + \lambda_t)\frac{\partial T_v}{\partial y}, \tag{4}$$

where μ_t and λ_t are given by a simple mixing length model. It is assumed that molecular transport processes are not significantly modified by the presence of droplets, so vapour phase values of λ and μ are used in Eq. (4). Likewise, values of λ_t and μ_t correspond to those of a single-phase turbulence model. These approximations are unlikely to incur serious error for the low values of wetness fraction considered here.

2.2. Formation and growth of the liquid phase

As fluid particles pass through the condensation zone, they experience variations in fluid properties and expansion rate which ultimately lead to the formation of droplets with a range of sizes. Accurate modelling of the condensation process requires retaining information on the whole spectrum of droplet sizes since smaller droplets have a higher surface area to mass ratio, and so respond more rapidly to changes in the flow properties. In the current calculations, the polydispersed nature of the liquid is modelled by retaining a number of droplet groups (typically 10–20 per decade of radius) at each point in the flow. Group i contains n_i droplets per unit mass of mixture, each of radius r_i, density ρ_i and at temperature T_i. The mass fraction of liquid per unit mass of mixture (the wetness fraction) is thus

$$y = \sum y_i = \sum \rho_i n_i 4\pi r_i^3/3, \tag{5}$$

where the summation is over all droplet groups. Neglecting the very small volume occupied by the liquid, the mixture density is given by $\rho = \rho_v/(1-y)$.

Similarly, the mixture specific enthalpy is

$$h = (1-y)h_v + \sum y_i h_i, \tag{6}$$

where h_v and h_i are the specific enthalpies of the vapour and group-i droplets, respectively. Since the vapour and liquid are not in general at equilibrium, ρ_v, h_v and h_i are not saturation values and must be evaluated at the temperatures and pressures corresponding to the relevant phase.

Once nucleation is complete, the absence of velocity slip guarantees that the number of droplets in each droplet group remains constant along streamlines. Changes in wetness fraction are therefore most conveniently calculated in a Lagrangian frame of reference. Recognising that new droplets are formed only at the critical radius and differentiating (5) following a fluid particle gives

$$\frac{Dy}{Dt} = (\rho_f \pi r_*^3/3)J + \sum 4\pi\rho_i n_i r_i^2 \frac{Dr_i}{Dt}, \tag{7}$$

where J is the nucleation rate, D/Dt is the substantive derivative (i.e., $\vec{u}\cdot\nabla$ for steady flow), and r_* is the Kelvin–Helmholtz critical radius. The theories of nucleation and droplet growth have been treated extensively in the literature and Young (1982) has shown that classical nucleation theory corrected for non-isothermal effects, combined with a slightly modified form of Gyarmathy's growth law give good agreement with extensive experimental data. The expressions adopted here for J, Dr_i/Dt and r_* are taken from the paper by Young. It is worth noting that both processes (and especially nucleation) depend strongly on the vapour subcooling, which is therefore a key parameter in determining phase change. In the present calculations, the subcooling is obtained from the enthalpy and pressure once the wetness fraction is known. Solution of the entire equation set therefore requires an iterative approach, as discussed below.

3. Numerical integration procedure

The momentum and energy equations may be cast in the form

$$\rho u \frac{\partial\phi}{\partial x} = S + \rho u \frac{\partial}{\partial\psi}\left(\alpha\rho u \frac{\partial\phi}{\partial\psi}\right)$$
$$\begin{cases} \phi = u, & \alpha = (\mu + \mu_t) \quad \text{momentum}, \\ \phi = h_o, & \alpha = (\lambda + \lambda_t)/c_{pv} \quad \text{energy}, \end{cases} \tag{8}$$

where S is a "source" term (defined below), c_{pv} is the vapour phase isobaric specific heat capacity, and ψ is the stream function defined by

$$\frac{\partial\psi}{\partial y} = \rho u \quad \text{and} \quad \frac{\partial\psi}{\partial x} = -\rho v. \tag{9}$$

The purpose of this transformation is to allow the use of a computational grid composed of streamlines ($\psi = \text{const.}$) and quasi-orthogonals ($x = \text{const.}$), as shown in Fig. 1. This greatly simplifies the Lagrangian style nucleation and droplet growth calculations and also maintains a more constant resolution of the growing boundary layer.

The source term for the momentum equation is simply the pressure gradient, $S = -dp/dx$, whereas for the energy equation S is derived by combining the definition of h_o with Eq. (6). After some manipulation, the result is

$$S = \rho u \frac{\partial}{\partial\psi}\left\{(1 - 1/Pr)u\tau + \frac{\lambda + \lambda_t}{c_{pv}}\rho u \frac{\partial}{\partial\psi}\sum y_i(h_v - h_i)\right\}, \tag{10}$$

where Pr is the (turbulent plus molecular) Prandtl number.

The solution proceeds downstream by integrating Eq. (8) from specified upstream profiles of u, v and h_o. The integration procedure follows broadly the finite volume scheme described by Cousteix (1988). Numerical stability is achieved by implicit discretization of the diffusive term in Eq. (8), using quantities at the downstream quasi-orthogonal, $i+1$ (Fig. 1). In an initial predictor step, the momentum equation is first solved to obtain the velocity profile on $i+1$, followed by the energy equation to give the stagnation enthalpy and temperature fields. This provides an initial guess of the subcooling which is used to integrate the nucleation and droplet growth equations along each streamline between i and $i+1$. The source term (Eq. 10) and mixture density are then updated and the procedure is repeated in one or more corrector steps. In practice, virtually no change occurs after the first correction.

Inlet profiles of u, v and h_o and the streamwise pressure distribution are specified as boundary conditions, and in all the calculations presented adiabatic and no-slip wall conditions have been used.

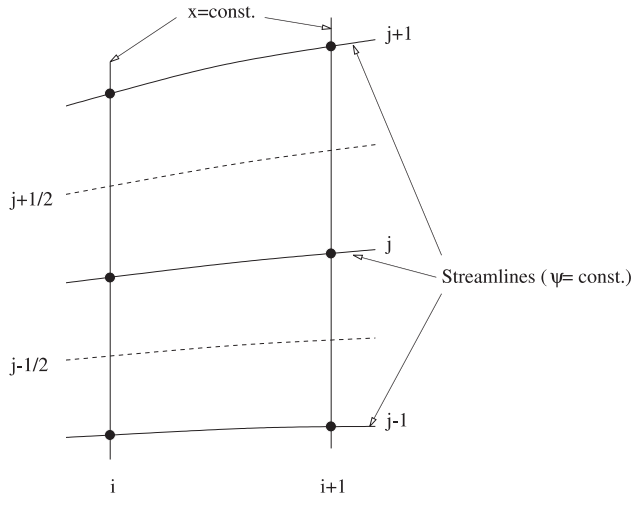

Fig. 1. Computational cell.

4. Results of calculations

The method was first validated in single-phase mode by computing standard test cases, including Blasius and Falkner–Skan profiles and turbulent flat-plate flow. In each case, excellent agreement was obtained with either the analytical solution or experimental data, but results are not presented here due to space constraints. Heat conduction aspects of the scheme were also tested by computing the adiabatic wall temperature recovery factor,

$$r = \frac{2c_{pv}(T_w - T_\infty)}{u_\infty^2},$$

at various Prandtl numbers. This was found to be in accord with the relation $r = Pr^{1/2}$ (Schlichting, 1979). Full condensing flow computations were then carried out using streamwise pressure distributions corresponding to a typical nozzle expansion. Since the equations solved are applicable only to a flat surface and no coupling is made with the 'outer' flow, the results may be viewed as valid only for thin boundary layers on the nozzle endwall. However, similar processes are likely to occur on the curved surfaces of turbine blades. Results for just one nozzle are presented, the geometry of which is given in Moore et al. (1973) where it is labelled as nozzle B.

The streamwise pressure distribution on the nozzle centreline was computed using an inviscid time-marching technique (White and Young, 1993), and is shown in Fig. 2 for flow with and without condensation. The pressure rise observed at $x = 0.1$ m is typical of wet supersonic expansions and is due to the release of latent heat at supersonic conditions. Unfortunately, no boundary layer data are available for this (or any other) condensing-steam nozzle flow. The boundary layer thickness was therefore arbitrarily set to 5 mm at $x = -0.05$ m (refer to Fig. 2), and both laminar and turbulent cases were investigated. Properties in the condensation zone were found to be relatively insensitive to the boundary layer profile at inlet, so a simple linear distribution of velocity together with constant h_o were specified. The grid density was typically 183 $\times$ 50 points ($x \times y$), spanning approximately two boundary

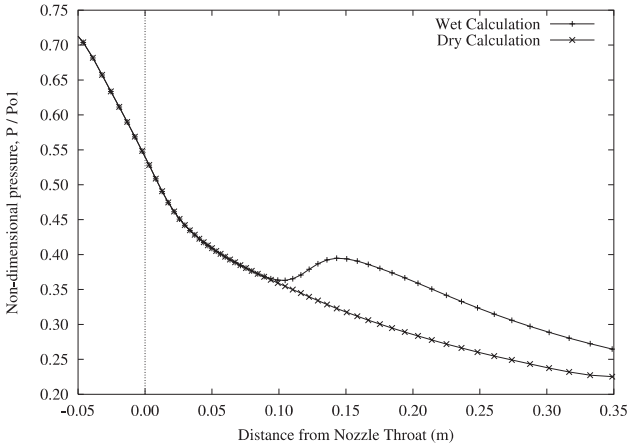

Fig. 2. Computed pressure variation along nozzle centreline.

layer thicknesses. Further refinement indicated grid independence.

The results presented below focus mainly on the laminar calculations since these exhibited a few additional features. In fact, the nature of the predicted phenomena was similar for the laminar and turbulent cases, with differences being mainly quantitative rather than qualitative.

4.1. Velocity profiles

The main impact of condensation upon inertial aspects of the boundary layer (velocity profiles, boundary layer thickness etc.) is likely to stem from the condensation pressure rise. Predicted velocity profiles at the end of this pressure rise ($x \approx 0.13$ m in Fig. 2) are shown in Fig. 3 for both laminar and turbulent cases. At this location, the calculated boundary layer thicknesses were 2.44 mm and 3.90 mm, laminar and turbulent, respectively. (For the turbulent calculations, the boundary layer was assumed fully turbulent from the inlet plane, $x = -0.05$ m.) As expected, the pressure rise has a substantially greater effect on the laminar boundary layer, which in the current case almost reaches separation: calculations carried out with the initial thickness, δ_{99}, in the range 0.5–50 mm gave typical reductions in the local skin friction coefficient of 80–90% for the laminar case but only 10–20% for the turbulent case.

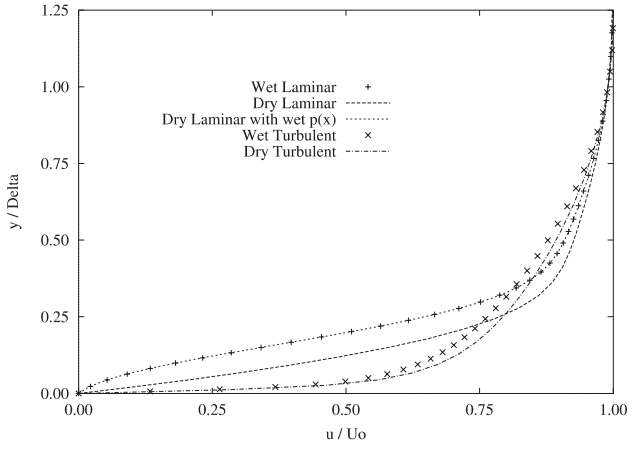

Fig. 3. Comparison of velocity profiles with and without condensation.

Fig. 3 also shows the laminar velocity profile computed with the pressure distribution corresponding to the wet expansion of Fig. 2, but with the condensation terms turned off. This is indistinguishable from the full condensing flow result, suggesting that velocity effects may be adequately modelled by combining an inviscid condensing flow calculation with a standard single-phase boundary layer method. (Inclusion of the wetness terms does, however, have a small effect on the predicted displacement and momentum thicknesses.)

Although the condensation process had little impact on the turbulent profile for the present nozzle expansion, the severity of the condensation pressure rise is dependent upon a number of factors, including the expansion rate and the location of the nucleation zone. Under certain circumstances, the heat release may be more than sufficient to revert the flow to sonic conditions (the so-called *supercritical* regime), in which case an aerodynamic shock-wave becomes embedded in the condensation zone (see, for example, Barschdorff and Fillipov, 1970). In such cases, the turbulent boundary layer may be more severely affected. (Numerical studies for supercritical moist air flow, conducted by Schnerr and Li (1933), suggest, however, that the shock-wave is considerably weakened at the boundary layer edge and does not initiate separation.)

4.2. Subcooling distribution

Plots of subcooling provide valuable understanding of how the condensation process varies across the boundary layer. Fig. 4 shows the predicted subcooling for laminar condensing flow. In the free stream, the expansion is fastest and is isentropic up to the point where nucleation begins. The subcooling in this region reaches a maximum of 36.6°C, giving extremely intense nucleation. The release of latent heat returns the flow rapidly to a near-equilibrium state, as seen by the abrupt collapse in subcooling and the subsequent equilibrium 'plateau'. Nearer to the nozzle wall, however, viscous dissipation maintains the temperature to within a few degrees of the initial stagnation value, so that as the pressure (and hence saturation temperature) falls, the steam becomes further superheated. A dry zone is therefore predicted in this region. In turbulent boundary layers, eddies are likely to carry droplets inward from the free-stream, but this effect has not been modelled in the present calculations.

At intermediate distances from the wall, the flow is sufficiently subcooled for nucleation to occur, but viscous dissipation and the relatively low expansion rate result in smaller departures from equilibrium than in the free stream. The lower values of subcooling give slower nucleation, providing substantially fewer droplets. Return to equilibrium is more grad-

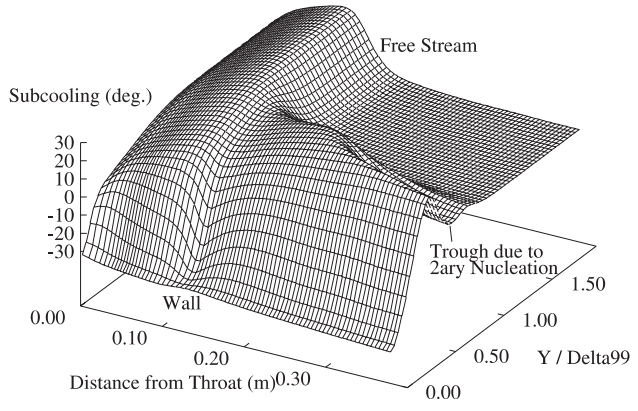

Fig. 4. Variation of subcooling for condensing laminar flow.

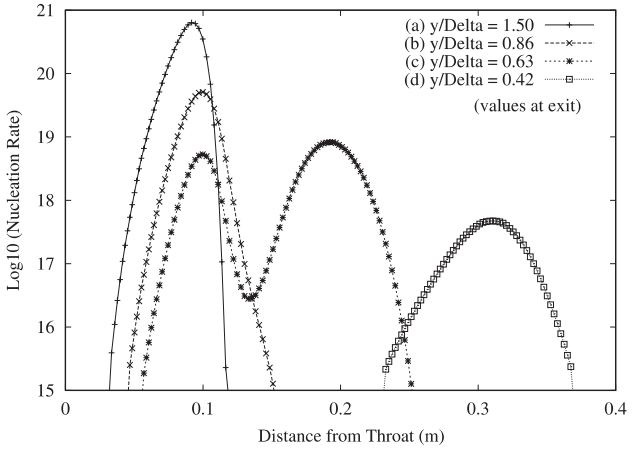

Fig. 5. Nucleation rate on different streamlines.

ual than in the free stream since less liquid surface is available for phase change.

The trough in subcooling midway through the boundary layer may be explained by reference to the plots of nucleation rate along individual streamlines, shown in Fig. 5. These indicate considerable variation across the boundary layer. In particular, on streamline *c* (corresponding to the trough of Fig. 4), the initial nucleation dies away due to a combination of dissipative heating and conduction from the hotter vapour on either side. Insufficient droplets are formed to prevent a further increase in subcooling as the flow continues to expand, and a second nucleation occurs further downstream. The large number of droplets nucleating in this downstream region in the neighbourhood of streamline *c* result in a rapid return to equilibrium, giving the observed trough of Fig. 4.

4.3. Wetness fraction and droplet sizes

Fig. 6 shows the distribution of wetness fraction for the above laminar flow calculation. The decrease in wetness and the postponed onset of condensation as the wall is approached are consistent with the isentropic efficiency of the expansion decreasing in this direction. The variation of wetness fraction across the nozzle exit is not monotonic since the the flow has not yet regained equilibrium. (Note that once equilibrium has been restored, the wetness depends only on the pressure and entropy.) Corresponding Sauter mean droplet radii (defined as three times the total volume of liquid per unit mass of mixture divided by the total surface area) are shown in Fig. 7, for which two interesting features are apparent. Firstly, secondary nucleation is evident as a small trough in the mean droplet size.

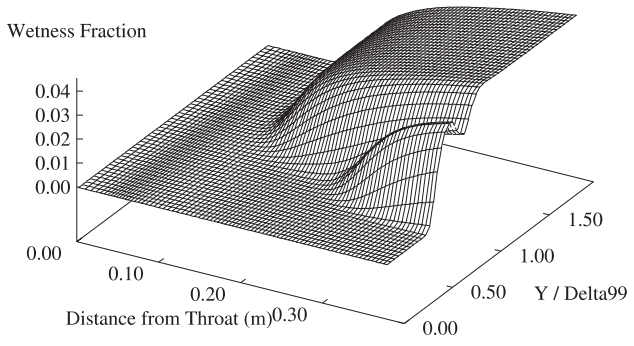

Fig. 6. Wetness fraction for condensing laminar flow.

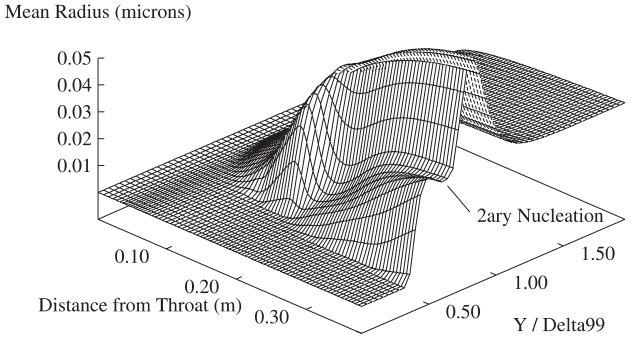

Fig. 7. Sauter mean droplet radii computed for laminar flow.

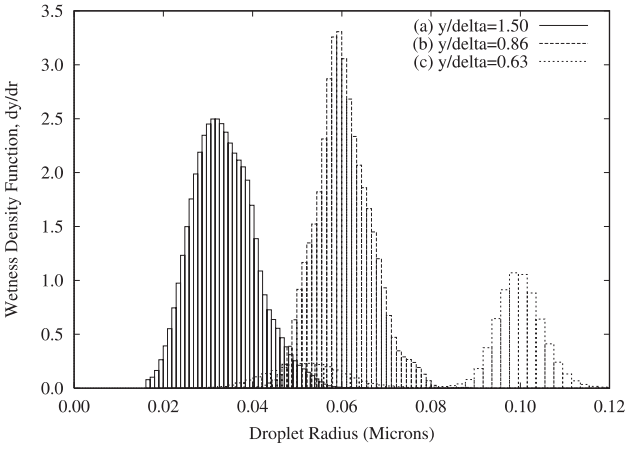

Fig. 8. Droplet size spectra on different streamlines.

This is because the formation of new, critically sized embryos tends to reduce the mean radius, counteracting the increase due to growth of established primary droplets. Secondly, the droplet size exhibits a maximum value close to the boundary layer edge (in this case at $y/\delta_{99} = 0.86$ at nozzle exit, coinciding with streamline *b* in Fig. 5). The occurrence of this maximum is in keeping with the results of Schnerr et al. (1992). It stems from the very small number of droplets nucleated on this streamline, which must grow to a larger size to attain the downstream equilibrium wetness fraction. The faster growth necessary to achieve this arises naturally by a slower decay of the subcooling, as seen in Fig. 4.

The above calculations were carried out whilst retaining up to 50 droplet groups per decade of radius. The resulting droplet size distributions at the nozzle exit plane, on three different streamlines, are shown in Fig. 8. The effect of secondary nucleation on streamline *c* is clearly to produce a bimodal size distribution, whilst the premature termination of nucleation on streamline *b* results in a distribution centred on a comparatively large radius. Since boundary layers for most practical condensing flow situations are likely to be very thin, optical droplet-sizing techniques, such as that developed by Walters (1973), would measure size distributions which are in some way averaged over the entire boundary layer. Fig. 9 shows the mass averaged droplet size distribution, obtained by weighting the wetness values with the increment in stream function associated with each streamline. Compared with the distribution in the free stream, droplet sizes are spread over a much wider range. The exact shape of this distribution will obviously depend on how much of the free stream flow is

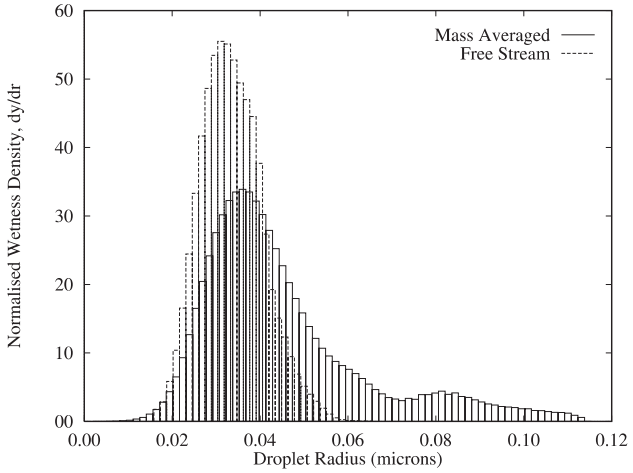

Fig. 9. Comparison of averaged and free stream droplet spectra.

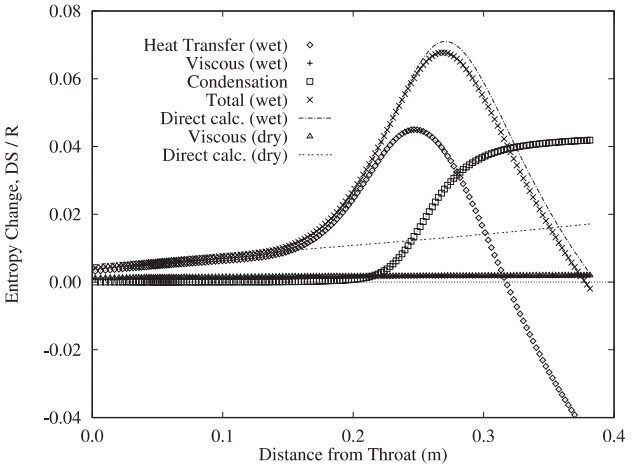

Fig. 11. Entropy changes along streamline (b).

included in the averaging, but it is nonetheless clear that boundary layer effects will be a contributing factor towards the broad droplet size spectra observed in steam turbine measurements (Walters, 1988).

4.4. Turbulent boundary layers

With the exception of the impact on velocity profiles, the turbulent calculations showed very similar trends to those described above. Fig. 10, for example, shows the distribution of predicted Sauter mean droplet radii. Although no secondary nucleation 'trough' is present, there is a peak in the mean droplet size part way through the boundary layer, similar to that observed in the laminar calculations. In this case, the peak occurs at $y/\delta_{99} = 0.56$, with a maximum radius almost three times the free stream value (the largest droplets being 0.17 μm in diameter). The practical significance of this feature with regard to steam turbine flows is that the larger droplets would considerably increase deposition of water onto blade surfaces. Due to so-called *turbophoretic* effects, transport of droplets by turbulent eddies is very sensitive to droplet radius in the predicted size range (Young and Leeming, 1997); a threefold increase in radius would conceivably enhance deposition by more than an order of magnitude, thereby exacerbating problems of blade erosion and increasing mechanical wetness losses.

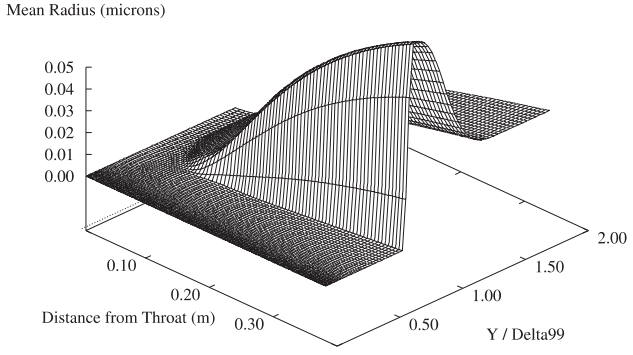

Fig. 10. Sauter mean droplet radii computed for turbulent flow.

4.5. Thermodynamic losses

One of the main concerns in wet-steam research is the significant reduction in turbine efficiency associated with condensation and it is thus of interest to examine how boundary layer losses are modified by phase change. An approximate derivation of the rate of entropy change following a fluid particle is presented in the appendix. The expression is composed of three terms, corresponding to viscous dissipation, heat transfer through the mixture, and irreversible phase change. Entropy changes due to the first and last of these processes are necessarily positive, whereas the second term may be either positive or negative according to whether the net heat flux is into or away from the fluid particle. Variations in entropy due to each of the processes are shown in Fig. 11 for streamline *b* (laminar calculations). Despite the level of approximation, the sum of the three contributions is in reasonable agreement with the entropy calculated directly using an expression similar to Eq. (6). One point of interest is that, following the onset of condensation, the heat transfer term becomes strongly negative. This is because the condensation heat release modifies the temperature profile such that there is a net transfer of heat away from fluid particles on this particular streamline. The entropy variation along streamline *b* for dry flow (using the same pressure distribution) is also plotted

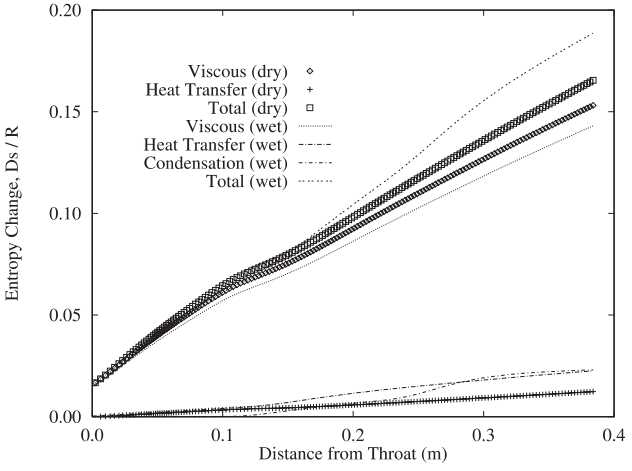

Fig. 12. Mass averaged entropy changes.

in the figure. In this case, the heat transfer term dominates (viscous dissipation is almost identical to the wet flow case) and the entropy monotonically increases.

Entropy changes from each of the processes described above vary considerably from streamline to streamline and it is of greater practical interest to consider mass-averaged values across the entire boundary layer. These are shown in Fig. 12 for both wet and dry laminar flow calculations. The presence of condensation causes a two-fold increase in the entropy rise due to heat transfer and adds a similar contribution due to irreversible phase change. However, since the viscous dissipation term dominates, the overall loss is similar for the wet and dry cases $\{(\Delta S/R)_{\text{wet}} = 0.19,\ (\Delta S/R)_{\text{dry}} = 0.17\}$. A similar result holds for turbulent flow calculations, for which the total losses were $(\Delta S/R)_{\text{wet}} = 0.34$ and $(\Delta S/R)_{\text{dry}} = 0.29$. Note that since an adiabatic wall condition has been used in all the calculations, the mass averaged entropy change due to heat conduction is always positive.

The distribution of loss between the three irreversible processes discussed above will clearly depend on the boundary layer thickness, the fraction of mass flow associated with the inviscid outer flow, and the state of the boundary layer. However, numerical experimentation over a range of thicknesses specified at inlet revealed that condensation itself is unlikely to change boundary layer losses by more than a few percent. Large aerodynamic losses due to separation, stemming from the condensation pressure rise, are nonetheless possible.

5. Conclusions

A numerical method for predicting the condensing flow of steam in boundary layers has been described and used to investigate the influence of viscous effects on condensation within a converging–diverging nozzle. Viscous dissipation and the reduced expansion rate within the boundary layer are seen to interact with the nucleation process in a complex manner, resulting in average droplet radii and size distributions which differ considerably from those predicted by inviscid flow. One feature, which occurs irrespective of the boundary layer state, is the formation of large droplets midway through the boundary layer due to premature termination of the nucleation process. Calculations with and without condensation suggest that the only major impact upon inertial aspects of the boundary layer (i.e., velocity profiles, skin friction etc.) is by virtue of the changed pressure distribution. Entropy generation rates have also been analysed and show that, although the details of loss generation are noticeably affected by condensation, the overall levels of loss are not substantially different.

Acknowledgements

The work described in this paper was carried out at the Laboratoire de Mécanique des Fluides et d'Acoustique at the Ecole Centrale in Lyon, France. The author gratefully acknowledges financial support received from The Royal Society.

Appendix A

A thorough analysis of the entropy production rate in condensing flow is a complex task requiring careful combination of the momentum and energy equations for the individual phases. For a formal derivation of entropy generation in inviscid gas-droplet flows, the reader is referred to Young (1995). For the present purposes, an approximate expression is sought which identifies entropy production due the various irreversible processes. Since the conservation Eqs. (1)–(3) are identical to their single-phase counterparts, they may be combined to derive entropy changes due to viscous dissipation and thermal conduction in a pure vapour. Multiplying Eq. (2) by u and subtracting from Eq. (3) yields

$$\rho u\frac{\partial h}{\partial x}+\rho v\frac{\partial h}{\partial y}-u\frac{\mathrm{d}p}{\mathrm{d}x}=\tau\frac{\partial u}{\partial y}-\frac{\partial q_y}{\partial y}. \tag{A.1}$$

Recognising that the flow is steady and that $\partial p/\partial y = 0$, and substituting for τ from Eq. (4) gives

$$\rho\frac{\mathrm{D}h}{\mathrm{D}t}-\frac{\mathrm{D}p}{\mathrm{D}t}=(\mu+\mu_{\mathrm{t}})\left(\frac{\partial u}{\partial y}\right)^2-\frac{\partial q_y}{\partial y}. \tag{A.2}$$

In the absence of condensation, changes in entropy may be written as $T_{\mathrm{v}}\,\mathrm{d}s = \mathrm{d}h - \mathrm{d}p/\rho$, so that Eq. (A.2) becomes

$$\frac{\mathrm{D}s}{\mathrm{D}t}=\frac{1}{\rho T_{\mathrm{v}}}\left\{(\mu+\mu_{\mathrm{t}})\left(\frac{\partial u}{\partial y}\right)^2-\frac{\partial q_y}{\partial y}\right\}. \tag{A.3}$$

This expression is not valid when condensation is occurring as the mixture then no longer has a single temperature, and additional terms due to phase transition must be included. Nonetheless, Eq. (A.3) may be taken as an approximation to entropy production due viscous and heat conduction effects, assuming these processes occur at the vapour temperature, T_{v}.

Due to the high specific enthalpy of phase change for water, entropy creation due to the condensation process itself is dominated by exchanges of heat between hot droplets and the surrounding subcooled vapour. This may be approximated by

$$\left(\frac{\mathrm{D}s}{\mathrm{D}t}\right)_{\text{cond.}}\approx\sum n_i q_i\frac{T_i-T_{\mathrm{v}}}{T_i T_{\mathrm{v}}} \tag{A.4}$$

(this relation can be obtained by neglecting terms due to momentum transfer, mass transfer and nucleation in the expression derived by Young (1995)). q_i is the heat transfer from a group-i droplet to the vapour, and equates approximately to the enthalpy of phase change

$$n_i q_i\approx(h_{\mathrm{v}}-h_i)n_i\frac{\mathrm{D}m_i}{\mathrm{D}t}\approx(h_{\mathrm{v}}-h_i)\frac{\mathrm{D}y_i}{\mathrm{D}t}. \tag{A.5}$$

Combining Eqs. (A.4) and (A.5) and assuming all droplets to be at the saturation temperature (a good approximation except in the very early stages of growth) gives

$$\left(\frac{\mathrm{D}s}{\mathrm{D}t}\right)_{\text{cond.}}\approx h_{\mathrm{fg}}\frac{\Delta T}{T_{\mathrm{s}}T_{\mathrm{v}}}\frac{\mathrm{D}y}{\mathrm{D}t}, \tag{A.6}$$

where h_{fg} is the specific enthalpy of phase change at saturated conditions. An approximate expression for the overall entropy production rate following a fluid particle is therefore

$$\left(\frac{\mathrm{D}s}{\mathrm{D}t}\right)\approx\frac{1}{\rho T_{\mathrm{v}}}\left\{(\mu+\mu_{\mathrm{t}})\left(\frac{\partial u}{\partial y}\right)^2-\frac{\partial q_y}{\partial y}\right\}+h_{\mathrm{fg}}\frac{\Delta T}{T_{\mathrm{s}}T_{\mathrm{v}}}\frac{\mathrm{D}y}{\mathrm{D}t}. \tag{A.7}$$

This consists of three terms corresponding to viscous dissipation, heat transfer and irreversible phase change, respectively.

References

Bakhtar, F., Heaton, A.V., 1988. An examination of the effect of wake chopping on droplet sizes in steam turbines. In: Technology of Turbine Plant Operating with Wet Steam, British Nuclear Energy Society, Thomas Telford, London, pp. 197–200.

Bakhtar, F., So, K.S., 1991. A study of nucleating flow of steam in a cascade of supersonic blading by the time-marching method. Internat. J. Heat and Fluid Flow 12, 54–62.

Barschdorff, D., Fillipov, G.A., 1970. Analysis of certain special operating modes of laval nozzles with local heat supply. Heat Transfer – Sov. Res. 2 (5), 76–87.

Cousteix, J., 1988. Couche Limite Laminaire: Aérodynamique. Collection La Chevêhe. Cepadues-Editions, Toulouse (in French).

Guha, A., Young, J.B., 1994. The effect of flow unsteadiness on the homogeous nucleation of water droplets in steam turbines. Phil. Trans. Roy. Soc. 349, 445–472.

Gyarmathy, G., 1963. On the growth rate of droplets in a supersaturated atmosphere. Z. Angew. Math. Phys. 14, 280–293 in German.

Moore, M.J., Walters, P.T., Crane, R.I., Davidson, B.J., 1973. Predicting the fog drop size in wet steam turbines. In: Wet Steam 4 Conf., Univ. of Warwick, Inst. of Mechanical Engineers (UK), Paper No. C37/73, pp. 101–109.

Schlichting, H., 1979. Boundary Layer Theory, seventh ed. McGraw-Hill, New York.

Schnerr, G.H., Bohning, R., Breitling, T., Jantzen, H.A., 1992. Compressible turbulent boundary layers with heat addition by homogeneous condensation. AIAA Journal 30 (5), 1284–1289.

Schnerr, G.H., Dohrmann, U., 1988. Theoretical and Experimental Investigation of 2D Diabatic Transonic and Supersonic Flowfields. In: Symp. Transonicum III (Götingen), IUTAM Symp., Springer, Berlin, pp. 132–140.

Schnerr, G.H., Li, P., 1933. Shock wave/boundary layer interaction with heat addition by non-equilibrium phase transition. Internat. J. Multiphase Flow 19 (5), 737–749.

Studziński, W., 1979. Boundary layer in compressible flow of wet water vapour. Internat. J. Multiphase Flow 5, 185–199.

Walters, P.T., 1973. Optical measurements of water droplets in wet steam. In: Wet Steam, Warwick, Vol. 4, pp. 32–40, Inst. Mech. Engrs., Paper C32/73.

Walters, P.T., Improving the accuracy of wetness measurements in generating turbines using a new procedure for analysing optical transmission data. In: Technology of Turbine Plant Operating with Wet Steam, pp. 207–215, London, 1988. British Nuclear Energy Society, Paper 27.

White, A.J., Young, J.B., 1993. Time marching method for the prediction of two-dimensional unsteady flows of condensing steam. AIAA Journal of Propulsion and Power 9 (4), 579–587.

White, A.J., Young, J.B., Walters, P.T., 1996. Experimental validation of condensing flow theory fora stationary cascade of steam turbine blades. Phil. Trans. Roy. Soc. 354, 59–88.

Young, J.B., 1982. The spontaneous condensation of steam in supersonic nozzles. Physico Chemical Hydrodynamics 3 (1), 57–82.

Young, J.B., 1995. The fundamental equations of gas-droplet multiphase flow. Int. J. Multiphase Flow 21 (2), 175–191.

Young, J.B., Leeming, A., 1997. A theory of particle deposition in turbulent pipe flow. J. Fluid Mech. 340, 129–159.